JACS
JOURNAL OF THE AMERICAN CHEMICAL SOCIETY

ARTICLE

pubs.acs.org/JACS

Peptide Synthesis in Aqueous Environments: The Role of Extreme Conditions and Pyrite Mineral Surfaces on Formation and Hydrolysis of Peptides

Eduard Schreiner,*[,†] Nisanth N. Nair,[‡] Carsten Wittekindt, and Dominik Marx

Lehrstuhl für Theoretische Chemie, Ruhr-Universität Bochum, 44780 Bochum, Germany

Supporting Information

ABSTRACT: A comprehensive study of free energy landscapes and mechanisms of COS-mediated polymerization of glycine via *N*-carboxy anhydrides (NCAs, "Leuchs anhydrides") and peptide hydrolysis at the water−pyrite interface at extreme thermodynamic conditions is presented. Particular emphasis is set on the catalytic effects of the mineral surface including the putative role of the ubiquitous sulfur vacancy defects. It is found that the mere presence of a surface is able to change the free energetics of the elementary reaction steps. This effect can be understood in terms of a reduction of entropic contributions to the reactant state by immobilizing the reactants and/or screening them from bulk water in a purely geometric ("steric") sense. Additionally, the pyrite directly participates chemically in some of the reaction steps, thus changing the reaction mechanism qualitatively compared to the situation in bulk water. First, the adsorption of reactants on the surface can preform a product-like structure due to immobilizing and scaffolding them appropriately. Second, pyrite can act as a proton acceptor, thus replacing water in this role. Third, sulfur vacancies are found to increase the reactivity of the surface. The finding that the presence of pyrite speeds up the rate-determining step in the formation of peptides with respect to the situation in bulk solvent while stabilizing the produced peptide against hydrolysis is of particular interest to the hypothesis of prebiotic peptide formation at hydrothermal aqueous conditions. Apart from these implications, the generality of the studied organic reactions are of immediate relevance to many fields such as (bio)geochemistry, biomineralization, and environmental chemistry.

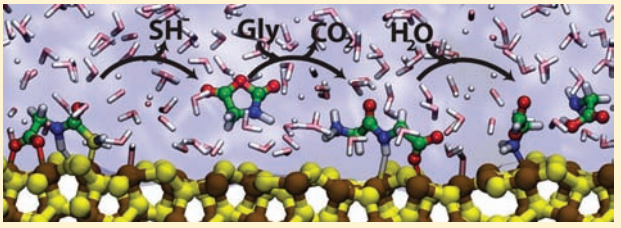

1. INTRODUCTION

The formation of peptide bonds is one of the most fundamental reactions in biology. Biological systems employ a sophisticated machinery to construct their proteins from amino acids: the majority of peptide bonds is formed in the ribosome, which translates genetic information into proteins. The ribosome catalyzes the aminolysis of an ester bond between the growing protein chain and a sugar by the next amino acid. Mechanistically, this reaction is a nucleophilic attack of an amino group of one amino acid at the activated carbonyl group of another amino acid. For the technical synthesis of peptides *N*-carboxy anhydrides (NCAs, also called "Leuchs anhydrides") proved to be useful as a form of activated amino acids.[1−4] NCAs show rich chemistry, both in organic solvents as well as in aqueous solution. In particular, the latter point makes NCAs interesting for the emerging field of "green chemistry".

Since NCAs can be synthesized from amino acids and simple inorganic compounds like NCO^-, NO/O_2,[5,6] or COS[7,8] in addition to chiral centers being preserved during NCA polymerization,[1] it has been suggested that NCAs may have played some role in prebiotic chemistry.[7−10] Interestingly, NCAs have been also proposed to be key components of the synthesis of nucleic acids[9,10] as well as peptides,[7,8] albeit the necessary reactions would occur at different conditions. This link extends the relevance of NCAs for prebiotic chemistry, addressing the coupling of the so-called "protein world" and the "RNA world" and thus the emergence of translation.[11]

Concerning the reaction conditions, it has been speculated that high pressures and temperatures like they occur at deep sea hydrothermal vents may facilitate peptide synthesis via an NCA pathway.[7,12] Additionally, it has been suggested that mineral surfaces, pyrite in particular, may have played a role during the prebiotic synthesis of peptides leading to the so-called "iron−sulfur world" (ISW) hypothesis.[13,14] In this "chemoautotrophic" hypothesis, surfaces of minerals like pyrite would allow for accumulation of reactants, thus increasing their local concentrations, act as catalysts, protect the products from the environment, and select molecules according their reaction times at those surfaces; see ref 15 for a recent review dedicated to adsorption and polymerization of amino acids on mineral surfaces. Indeed, several experimental works provide evidence for the feasibility of peptide synthesis at high temperatures and pressures[16] and at transition metal sulfides,[7,8] the latter suggesting interesting chemical reaction cycles with NCAs at their core. Both NCA activation and pyrite minerals have been proposed to be potentially involved in the prebiotic aqueous

Received: December 21, 2010
Published: May 11, 2011

dx.doi.org/10.1021/ja111503z | *J. Am. Chem. Soc.* 2011, 133, 8216–8226

synthesis not only of peptides but also of nucleic acids.[17,18] Apart from the relevance for the origin of life research, interactions of biomolecules with wet mineral surfaces and organic reactions at aqueous mineral interfaces, including high-temperature and -pressure conditions, are of crucial importance in fields ranging from (bio)geochemistry to biomineralization to environmental chemistry.

Iron pyrite, FeS_2, is an abundant sulfide mineral in the earth's crust. Due to its importance in other fields, especially environmental chemistry and (bio)geochemistry, the highly exposed $FeS_2(100)$ surface has been intensely investigated using various experimental techniques.[19−23] Theoretical investigations contributed unique insights into the electronic structure of bulk pyrite and different surfaces[24−33] including our understanding of molecular/dissociative adsorption/desorption of small molecules on pyrite.[33−40] It is important to note that the relatively high reactivity of naturally occurring pyrite is attributed to a typically high concentration of sulfur vacancies on its fractured (100) surface.[19,41,42] Furthermore, such sulfur vacancies are the most prominent type of defects of pyrite surfaces apart from steps and terraces.[43,44] The resulting undercoordinated iron atoms at these point defects are expected to show interesting effects in adsorption of molecules on pyrite and the chemical reactivity of its "real" surfaces.

In order to understand the reaction mechanisms involved in the NCA-mediated activation and polymerization of amino acids and the impact of geophysical conditions like pressure, temperature, and the presence of mineral surfaces, it is necessary to investigate these reactions at the molecular level. An experimental challenge for the study of chemical reactions in the realm of (bio)geochemistry is the extreme thermodynamic conditions that need to be considered. Hydrothermal vents, in particular, are known to be a favorable environment for a wealth of biogeochemical processes at aqueous conditions where the conditions correspond to aqueous solutions at typically $T \approx 500$ K and $p \approx 20$ MPa (see refs 45−47 for instance). As an increasingly powerful complement to experiment, numerical simulations based on density functional theory have proven to yield unique and valuable insights into interactions of biomolecules with mineral surfaces.[33,48−51] However, such calculations are often restricted to total energy calculations of static optimized structures thus lacking temperature effects and entropic contributions to the free energy being most relevant in aqueous solutions where properties are known to change dramatically as a function of temperature and/or pressure.[52] Molecular dynamics simulations based on density functional theory, on the other hand, offer a unique opportunity to study complex chemical reactions at controlled (and even extreme) conditions taking into account finite temperatures, elevated pressures, entropy effects, solvation phenomena, and last but not least surface catalysis on an equal footing.

The first set of such ab initio molecular dynamics (AIMD) simulations[53] at hypothetical ISW conditions were performed not that long ago.[34] Studying the adsorption of the amino acid glycine at an ideal pyrite (100) surface, the authors found that at conditions resembling hydrothermal environments (i.e., hot-pressurized water at the pyrite interface (PIW) on the (100) face of FeS_2 where $T = 500$ K, $p \approx 20$ MPa) glycine adsorbed in a monodentate mode but readily desorbs within picoseconds only. A bidentate adsorption mode has been shown to improve the retention times only marginally in the context of chemical reactivity at water/mineral interfaces.[39] In a follow-up study,

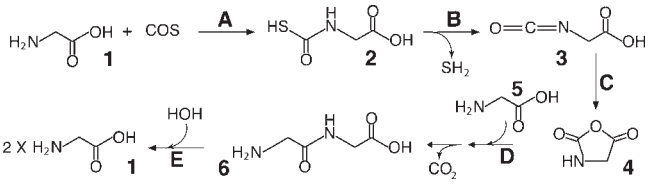

Figure 1. Sequence of reaction steps investigated in this study leading from glycine and COS to diglycine at extreme temperature and pressure conditions (see text) as well as its hydrolysis in the last step E. All individual reactions were studied at water−pyrite interfaces (PIW, using ideal and defective surfaces omitted for clarity at this stage) and, for reference, in bulk water at the same thermodynamic conditions.

the impact of sulfur vacancies on the desorption mechanism and desorption free energies of glycine at wet defective (100) pyrite surfaces was addressed.[40] This study made clear that sulfur vacancies at the pyrite surface can increase the retention times of glycine by up to nine (!) orders of magnitude.

Recently, we investigated the activation of amino acids to NCAs by COS[54,55] and the subsequent reaction of NCAs with amino acids to form peptides in *bulk* aqueous solutions.[54,56] These works have elucidated the impact of high temperature and pressure on the reaction mechanisms involved as well as their free energies at bulk solvation conditions. Importantly, findings were that the extreme conditions (denotes as hot-pressurized bulk water and abbreviated by "HPW") not only speed up reactions due to the higher temperature but also shift the equilibrium between charged and neutral molecular species by *stabilizing the latter*.[55] This shift in equilibrium has been shown to alter reaction mechanisms as compared to ambient solvation conditions. At both ambient and extreme thermodynamic conditions hydrolysis of the peptide bond is slower than the synthesis, suggesting that an accumulation of peptides is possible at both conditions.[56] Additionally, it was found that the formation of NCA from an amino acid and COS takes a route via isocyanate, which is more preferred than a direct cyclization of the *N*-thiocarboxyl amino acid ("thiocarbamate pathway").[55]

The purpose of the present study is to address in detail the role a pyrite mineral surface, both ideal (100) and defective via sulfur vacancies, is playing in some of the key reactions of the previously examined peptide cycle at extreme conditions.[54−56] This requires one to investigate many distinct elementary steps in this work which are summarized and labeled in Figure 1 in addition to some side reactions that have been studied in passing. Thus, the emphasis of this paper is exclusively on the possible impact of a wet mineral surface on the reaction mechanism of elementary synthesis steps that lead from glycine to diglycine, including straightforward hydrolysis, according to the sequence sketched in Figure 1.

2. METHODS AND MODELS

The setup of the present AIMD simulations as well as the used methodology were chosen close to those used in our previous works[34,39,40,54−56] and thus need to be described only briefly here.

All calculations were performed within the spin-restricted Kohn−Sham density functional theory in its plane wave/pseudopotential formulation.[53] The PBE[57,58] exchange-correlation functional was chosen, and the core electrons were taken into account using Vanderbilt's ultrasoft pseudopotentials.[59] The pseudopotentials contained additional *d* projectors in the case of sulfur and scalar relativistic corrections as well as semicore states for iron. A plane wave cutoff of 25 Ry was used since it was

sufficient to obtain convergence in the unit cell parameter and S−S distance of pyrite.[40] More details of the benchmark calculations can be found in ref 39. The AIMD simulations[53] were performed using the Car−Parrinello scheme[60] together with Nosé−Hoover chain[61] thermostats for nuclei and electronic orbitals. A time step of 0.145 fs was used for integration of the equations of motion, and the fictitious mass for the orbitals was 700 au. To maintain an adiabatic separation between nuclear and electronic degrees of freedom for the chosen time step and orbital mass, the hydrogen atoms in the system were substituted by deuterium atoms.

The three-dimensional periodic boundary conditions employed in our simulations establish a lamella of water between the upper and the lower faces of the pyrite slab. The simulations were carried out in an orthorhombic box with dimensions 10.8 × 10.8 × 18.9 Å^3 containing 36 water molecules in contact with a slab of pyrite. The system was thermostatted to 500 K, which results in an expected pressure of about 20 MPa in accordance to PIW thermodynamic conditions; this setup results in a water density of ∼0.85 g/cm^3 according to ref 62. The pyrite slab exposed the (100) surface comprised of 9 atomic layers with 24 Fe and 48 S atoms in total. During all calculations the three atomic layers opposite to the face with adsorbed organic molecules were kept fixed at their bulk positions. At all these simulation conditions, introduction of an organic molecule like glycine or NCA replaced a water molecule, thus approximately maintaining the water density. The initial equilibrated structures of the systems were obtained as the result of a previous reaction step or by employing a multistep equilibration protocol as outlined earlier.[55,56]

In order to compute free energy profiles of the studied reactions in solution at an interface the continuous extended Lagrangian formulation[63] of ab initio metadynamics[64] was used as implemented in the CPMD simulation package.[65] This strategy has been proven[40,54−56] successful for the sort of complex problem investigated here with an accuracy of estimated free energy barriers of ∼1 k_BT. In order to sample multidimensional reaction free energy surfaces more efficiently the so-called "multiple walker" algorithm[66,67] has been employed in some cases. Several replicas of the system, which are called walkers, fill the same free energy surface simultaneously since each of these walkers moves on the sum of the biasing potentials added by all walkers. We designed an efficient parallel implementation of this algorithm tailored for Blue Gene/P platforms used here, which yields linear scaling with the number of walkers.[66] By virtue of this implementation we were able to use many thousands of processors which resulted into a dramatic speedup for sampling the multidimensional free energy surfaces. Typically, we used between four and eight replicas with each of them running on 4096 cores on a Blue−Gene/P platform.[67] In all cases different replicas were initialized using different initial velocities but using the same initial positions. In order to avoid so-called "hill-surfing" problems[68] we have taken special care that replicas do not add biasing potentials simultaneously within a radius of 1.5 times the width of the Gaussian biasing function.

3. RESULTS AND DISCUSSION

3.1. Reaction of Glycine with Carbonyl Sulfide. Having in mind to capture the chemically relevant free energy subspace which must host the reaction coordinate, we chose two very general collective coordinates, being high-dimensional themselves in the sense of the number of underlying Cartesian coordinates defining them. The first one is the coordination number of the nitrogen atom of glycine to *all* nonaliphatic hydrogen atoms in the system, $c[N_{Gly}-H_{na}]$, whereas the second one is the distance between this nitrogen atom and the carbon atom of COS, $d[N_{Gly}-C_{COS}]$. A repulsive wall potential was set for the former coordinate such that the value of this coordinate is not allowed to increase beyond 1.9 to avoid sampling other

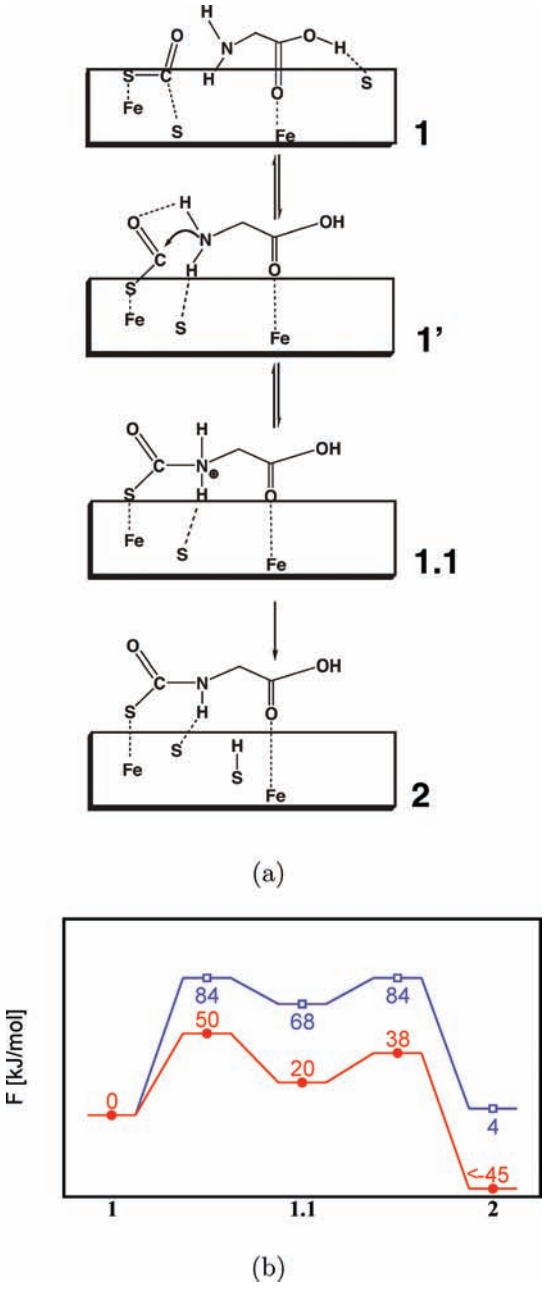

Figure 2. (a) Mechanism for the reaction of glycine with COS at the water−pyrite interface at extreme thermodynamic conditions (PIW, see text). (b) Free energy profile along the minimum free energy pathway at the water−pyrite interface at extreme thermodynamic conditions (PIW, red line and filled circles) and in hot-pressurized bulk water at the same conditions (HPW, blue line and open squares). Note that b and thus a are derived from two-dimensional free energy surfaces (see Figure S2, Supporting Information).

protonation states of N_{Gly}. The total mechanism of the reaction along route A (according to the scheme presented in Figure 1) at PIW conditions and the free energy profiles at both PIW and HPW conditions are depicted in Figure 2 (the corresponding full free energy surface is presented in the Supporting Information, see Figure S2). In the starting configuration carbonyl sulfide, COS, is adsorbed via its carbon and sulfur atoms to a sulfur and an iron atom of the surface, respectively. Concerning the adsorption of the glycine molecule on the surface a bidentate mode **1** via the

dx.doi.org/10.1021/ja111503z |J. Am. Chem. Soc. 2011, 133, 8216–8226

carboxyl group was chosen given our previous finding that a monodentate adsorption mode is quite unstable in the sense of being characterized by short retention times at least at PIW conditions.[34]

During the simulation the glycine amino group hydrogen atoms form hydrogen bonds with both O_{COS} and S_{surf}. The caused weakening of the $C_{COS}-S_{surf}$ bond allows the carbon to detach from the surface, leading to the arrangement **1′**. Subsequently, **1.1** is formed by a direct nucleophilic attack of N_{Gly} on C_{COS}. The barrier for this step is 50 kJ/mol at PIW conditions (corresponding to 12 k_BT_{500} in terms of thermal energy units at this elevated temperature), which is 8 k_BT_{500} lower than in HPW.[55] The reason for this lowering in free energy barrier compared to the situation at HPW conditions is seen in the decrease of entropic contributions due to the immobilization of the reactants: they are adsorbed at the surface and unlike in a bulk situation cannot arbitrary reorient themselves with respect to each other. Thus, the number of available conformations the reactants can adopt relative to each other is expected to be lower for adsorbed reactants. This is a genuinely geometric (or "steric") effect arising when the accessible reaction environment is reduced from three to two dimensions and thus should be generic to all surfaces.

The resulting adduct **1.1** is the same as that observed in the bulk water simulations (species **1.1** in ref 55), but at PIW conditions it is attached to the mineral surface via the carboxyl and the COS groups. In the subsequent deprotonation step the proton is transferred directly without any water assistance from the nitrogen atom to one of the surface sulfur atoms with a barrier of 18 kJ/mol (i.e., 4 k_BT_{500}). Note that upon increasing the relaxation time the glycine molecule desorbs from the surface, indicating that in reality the glycine concentration at the *ideal* pyrite surface is expected to be rather low.

To economize on simulation time no complete sampling of the product free energy basin was attempted at PIW conditions, but it can be safely concluded that the product is at least 45 kJ/mol more stable than the reactants. This increase in stability of the product as compared to the bulk situation[55] is due to the fact that **2** stays adsorbed at the surface: S_{COS} and O_{Gly} both bind to iron atoms and, more importantly for the stability of **2**, the hydrogen atom at the nitrogen site forms a hydrogen bond with one of the surface sulfur atoms. This adsorption mode causes **2** to orient slanted with respect to the surface. Thus, one side of the thiocarbamate group is completely screened from water by the surface, thereby preventing a protonation of the nitrogen atom. Note that due to the adsorption no proton exchange is observed at the COS and carboxyl groups as described earlier for the situation in bulk water.[55]

Taking into account the data reported earlier in ref 55 for the bulk solvation regime, the rate-limiting step for the formation of *N*-thiocarboxyl amino acid in ambient bulk water, in both HPW and PIW conditions, is the nucleophilic attack of the amino group on COS. The total activation barrier in the present case is 12 k_BT_{500} at PIW conditions, whereas the barrier was calculated previously to be 20 k_BT_{500} at bulk solvation conditions in HPW.[55] Compared to the previous studies in bulk solution[55] the pyrite surface does not qualitatively change the reaction mechanism as such. However, the mineral surface has a quantitative influence in that it does speed up the reaction by both lowering the entropic contributions to the reactant well and stabilizing the product due to screening it from water. In addition, the pyrite surface does influence the details of the mechanism by playing the role of a proton acceptor, thus replacing water in this respect.

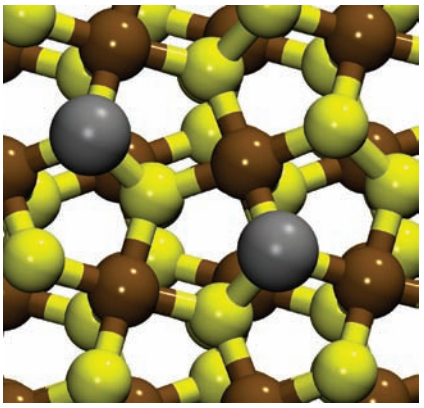

Figure 3. Pyrite slab, $Fe_{24}S_{46}$, viewed down the surface normal to its active face, used to represent the defective $FeS_2(100)$ surface. Yellow and brown spheres represent sulfur and iron atoms, respectively, whereas the gray spheres represent the sulfur atoms removed from the ideal surface to create the two sulfur vacancy defects.

3.2. Formation of NCA. As demonstrated earlier[55] the formation of NCAs from *N*-thiocarboxyl amino acid prefers to pass through the formation of an isocyanate carbonic acid species, which further reacts to NCA through an intramolecular cyclization (see route B in Figure 1). It is conceivable that surfaces, such as that of pyrite, might change the mechanism to a direct cyclization pathway of *N*-thiocarboxyl amino acid to NCA. At PIW conditions a S-deprotonated thiocarbamate, which was adsorbed via the sulfur atom at the surface, was chosen as the starting configuration. Such an adsorption mode is expected to be stronger than that used previously.[34] However, as soon as the sulfur atom becomes protonated, the thiocarbamate is found to desorb readily from the pyrite surface, and thus, no direct cyclization could be observed subsequently. This implies that on the ideal pyrite (100) surface no alternative mechanisms exist, which would allow direct formation of NCA from *N*-thiocarboxyl amino acids on the time scale of desorption for this particular reactant on that surface at these solvation conditions.

The mechanism of isocyanate formation in bulk aqueous solution[55] clearly shows that the protonation of the sulfur atom is essential for this reaction step, and thus, it cannot be circumvented, at least not on an ideal pyrite surface. As described for the case of direct cyclization of a thiocarbamate, it can be expected that the thiocarbamate will desorb from the ideal (100) surface upon protonation of the sulfur atom. On the basis of these observations together with our experience gained with glycine desorption from both ideal and defective pyrite surfaces,[34,39,40] we decided to investigate the isocyanate formation on a defective FeS_2 surface instead of on its ideal (100) face.

3.2.1. Sulfur Divacancy Model. From our earlier studies[40] it can be concluded that more than one defect is necessary to keep the reactants on the surface on sufficiently long time scales. Thus, as a first step we obtained a stable structure of a pyrite surface with two sulfur vacancies. Structures having different distributions of two sulfur vacancies on the surface were constructed, and geometry optimizations of these structures were performed in singlet, both closed and open shell, and quintet electronic states. The divacancy structure shown in Figure 3 has the lowest potential energy. As already found for the case of a single sulfur vacancy by us and confirmed by others,[33,40] in the ground state of the divacancy pyrite slab the electrons are seen to be fully paired

dx.doi.org/10.1021/ja111503z | J. Am. Chem. Soc. 2011, 133, 8216–8226

to yield a closed-shell electronic configuration. Upon breaking S−S dimer bonds on the surface by formation of a sulfur vacancy, the associated electrons are being localized on the S atom remaining on the surface itself, formally becoming a $S^{2-}$with a lone pair of electrons directed toward the vacancy. Checking for the stabilities of both higher multiplicities within open-shell calculations and alternative divacancy configurations yielded total energies that are roughly 23 and 20 kJ/mol higher, respectively. Therefore, the structure depicted in Figure 3 was used in the subsequent simulations of isocyanate formation, **3**, from the thiocarbamate **2** at the pyrite−water interface in the presence of two sulfur vacancies.

3.2.2. Formation of Isocyanate. Several adsorption modes of **2** at the defective pyrite surface with its sulfur divacancy (see Figure 3) were investigated. In the following, we only present two cases in which the reaction led to isocyanate **3**.

Adsorption Mode A. One particularly favorable adsorption mode of thiocarbamate **2** in the presence of two surface sulfur vacancies is shown in Figure 4a. Here, both carboxylate oxygens and the sulfur atom are coordinating three different Fe atoms close to a defect site. Note that **2** is set up in a different protonation state compared to **2** in Figure 2. This adsorption mode is expected to be very stable since both the oxygen and the sulfur atoms are binding to undercoordinated iron atoms neighboring the sulfur vacancy. Additionally, the N−H group forms a hydrogen bond with a three-fold-coordinated surface sulfur atom. After 5 ps of canonical AIMD simulation at PIW thermodynamic conditions this structure remained stable on the surface. In order to bias possible reaction mechanisms least a four-dimensional reaction space was spanned in order to sample the free energy landscape and thus to study the reaction mechanism of thiocarbamate **2** to isocyanate **3**. In particular, the reaction space was spanned by the coordination number of the carbon to the sulfur atom, both from the thiocarbamate group, $c[C_{COS}-S_{COS}]$, the coordination number of the nitrogen atom to *all* nonaliphatic hydrogen atoms in the system, $c[N-H]$, the coordination number of the sulfur atom of the thiocarbamate group to *all* nonaliphatic hydrogen atoms in the system, $c[S_{COS}-H]$, and the coordination number of the oxygen atom of the thiocarbamate group to *all* nonaliphatic hydrogen atoms in the system, $c[O_{COS}-H]$.

The total reaction mechanism is similar to that observed earlier at HPW conditions:[55] deprotonation at the nitrogen atom followed by an elimination of SH^-. However, unlike in bulk solution, no reaction channels involving a deprotonation at the sulfur was observed at interfacial conditions. Furthermore, a two-dimensional cut at $c[O_{COS}-H] = 0.3$ and $c[S_{COS}-H] = 1.0$ (see Figure S3, Supporting Information) shows that the rate-determining step for this particular reaction is *not* the breakage of the C−S bond as in the HPW bulk case[55] but the deprotonation at the nitrogen at PIW conditions. The free energy barrier for this step is 115 kJ/mol, which is 19 kJ/mol higher than in solution; note the pyrite surface acts as proton acceptor here. Once the proton is transferred to the surface the C−S bond readily breaks (13 kJ/mol or about 3 k_BT_{500}), forming the isocyanate **3**. In contrast to the HPW bulk solution no SH_2 is formed at PIW conditions but $SH^-$and $H^+$are adsorbed to the pyrite surface. This implies that the mineral surface, instead of water itself, acts as both proton and SH^-acceptor.

Overall, the effective free energy barrier for this interfacial reaction is 122 kJ/mol (29 k_BT_{500}), which is 33 kJ/mol (8 k_BT_{500}) lower than at HPW conditions.[55] This result clearly indicates that the defective surface can have an accelerating effect on the formation of isocyanate with respect to the same reaction in bulk water at the same thermodynamic conditions being the proper reference.[55] Three observations are important regarding the influence of the pyrite surface on the observed reaction. First, the surface excludes some of the reaction channels observed in solution. Second, the surface is not just an "inert wall" but chemically involved in the reaction. Third, the screening of the thiocarbamate from water increases the barrier for the deprotonation at the nitrogen with respect to the situation in bulk at the same conditions.

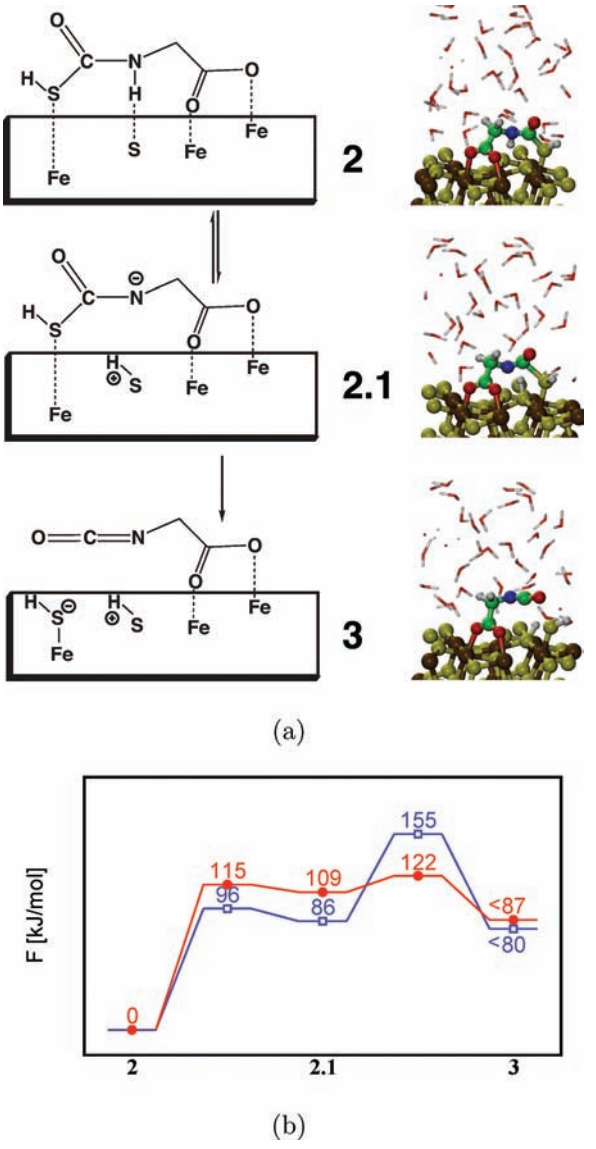

Figure 4. (a) Mechanism for isocyanate formation at the defective pyrite surface (see Figure 3) at extreme thermodynamic conditions (PIW) together with representative snapshots extracted from the ab initio metadynamics simulation. Color code: red (oxygen), green (carbon), white (hydrogen), blue (nitrogen), yellow (sulfur), and brown (iron). (b) Free energy profile along the minimum free energy pathway for the formation of isocyanate at the water−pyrite interface at extreme thermodynamic conditions (PIW, red line with filled circles) and in hot-pressurized bulk water at the same conditions (HPW, blue line and open squares). Note that b and thus a are derived from four-dimensional free energy surfaces (see Figure S3, Supporting Information, for a two-dimensional cut at $c[O_{carbox}-H] = 0.3$ and $c[S_{COS}-H] = 1.0$).

dx.doi.org/10.1021/ja111503z |*J. Am. Chem. Soc.* 2011, 133, 8216–8226

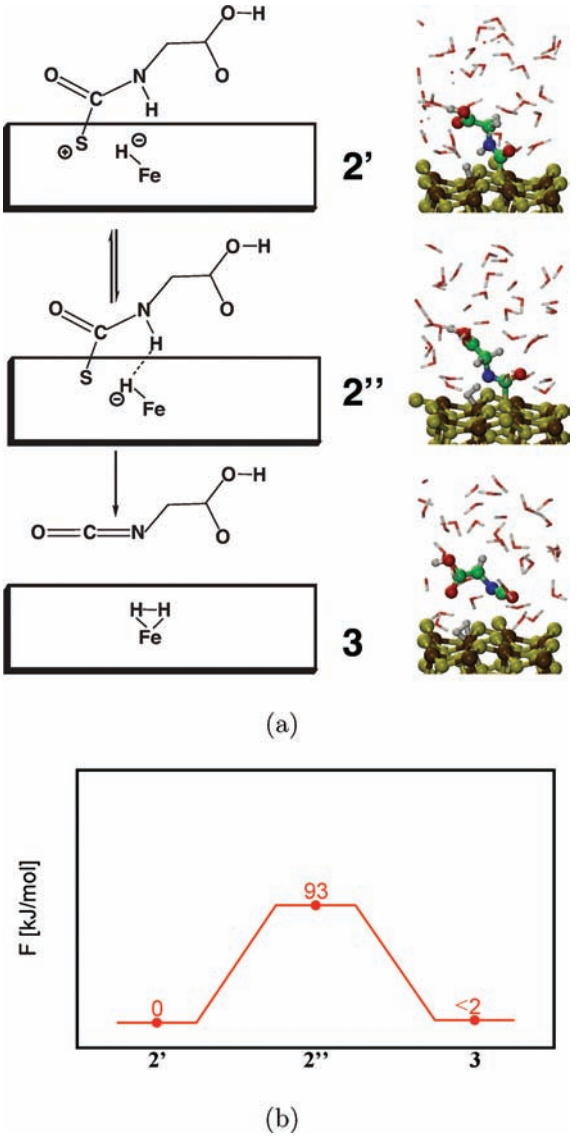

Figure 5. (a) Mechanism for isocyanate formation at the defective pyrite surface (see Figure 3) at extreme thermodynamic conditions (PIW) together with representative snapshots extracted from the ab initio metadynamics simulation. This mechanism was observed for the constructed adsorption mode shown in the topmost snapshot (adsorption mode B). Color code: red (oxygen), green (carbon), white (hydrogen), blue (nitrogen), yellow (sulfur), and brown (iron). (b) Free energy profile along the minimum free energy pathway at the water−pyrite interface at extreme thermodynamic conditions (PIW, red line and filled circles). Note that b and thus a are derived from four-dimensional free energy surfaces (see Figure S4, Supporting Information, for a cut along $c[C_{COS}-H^-] = 0.25$).

Adsorption Mode B. Using the starting structure in Figure 5a, we investigated the possibility of a hydride-mediated proton abstraction from the N−H group. In this adsorption mode, only the S atom binds to the vacancy on the surface and the hydrogen atom from the thiocarbamate sulfur is adsorbed at an iron atom close to the defects as a hydride. Since H^- is a stronger base than the 3-fold-coordinated surface sulfur atoms, abstraction of the N−H proton is expected to be much easier as in the previously described case. Moreover, the C−S bond is weaker compared to the situation in the thiocarbamate molecule due to the bonding of the sulfur atom of thiocarbamate with Fe and S surface sites as seen from the topmost snapshot in Figure 5a.

In order to simulate the formation of isocyanate for this adsorption mode a four-dimensional reaction space was again chosen: the coordination number of the carbon to the sulfur atom, both stemming from the thiocarbamate group, $c[C_{COS}-S_{COS}]$, the coordination number of the nitrogen atom to *all* nonaliphatic hydrogen atoms in the system, $c[N-H]$, the coordination number of the hydride to *all* nonaliphatic hydrogen atoms in the system, $c[H^- - H]$, and the coordination number of the carbon atom of the thiocarbamate group to the hydride $c[C_{COS}-H^-]$. Note that the last collective coordinate takes into account the possibility that the hydride could move to the thiocarbamate/isocyanate carbon atom.

As shown in Figure 5a, the reaction proceeds by a concerted transfer of the N−H proton to the hydride, thus forming an H_2 molecule and breaking the C−S bond. The free energy barrier for this process is about 22 k_BT_{500} (93 kJ/mol) at PIW conditions, which is much lower than the barrier for this step in HPW (37 k_BT_{500}). The final significance of this route is not fully clear yet as for conclusive statements one would have to compute the free energy barriers for adsorption of thiocarbamate at the surface sulfur vacancy accompanied by hydride transfer to surface iron in addition. However, the observed mechanism does represent an interesting, albeit admittedly exotic, alternative to that described in the previous section.

The above mechanism is similar to the disulfide intermediate pathway pointed to by Leman et al.[8] According to these earlier findings, in the presence of an oxidizing agent, thiocarbamate is able to dimerize to bisaminoacyl thiocarbamate disulfides, which subsequently undergo a transition metal driven cyclization to NCAs. The initial adsorption structure in Figure 5a has a S−S bond, between that of a thiocarbamate and a three-fold-coordinated (second layer) surface S. By the formation of isocynate, the C−S bond is broken, leaving the S atom at the surface, similar to the S_2^{2-} elimination proposed in ref 8.

3.2.3. Cyclization of Isocyanate. For the cyclization of the isocyane carbonic acid (corresponding to route C in Figure 1) the deprotonated isocyanate was adsorbed in a bidentate mode **3** via the carboxylate oxygen atoms to iron atoms near a sulfur vacancy defect. For this reaction a pyrite surface containing only one sulfur vacancy was used. This defect does not play an active role in the reaction, but it is expected to stabilize the adsorption of isocyanate at the surface according to what has been observed earlier in the case of glycine.[40]

To capture the relevant reaction space and to ensure direct comparability with previous work the same collective coordinates were chosen as in the bulk HPW simulations,[55] namely, the distance between the carbon atom of the isocyanate group and an oxygen atom of the carboxyl group, $d[C_{iso}-O_{carbox}]$, and the coordination number of the nitrogen atom with respect to *all* nonaliphatic hydrogen atoms, $c[N-H_{na}]$. During the reaction $d[C_{iso}-O_{carbox}]$ should decrease and $c[N-H_{na}]$ should increase from zero to approximately unity. On the basis of our experience from the investigation of the direct cyclization of thiocarbamate in bulk water, HPW, we followed ref 55 and added repulsive wall potentials when $d[C_{iso}-O_{carbox}] > 4.3$ Å and $c[N-H_{na}] > 1.4$.

The reaction mechanism and the free energy profile are shown in Figure 6 (for the reconstructed free energy surface see Figure S5, Supporting Information). At the pyrite−water interface the same key mechanistic steps are observed as in the bulk solution,[55] but in the present case the pyrite surface clearly acts as a catalyst in the sense of heterogeneous catalysis at liquid−solid interfaces.

dx.doi.org/10.1021/ja111503z |*J. Am. Chem. Soc.* 2011, 133, 8216–8226

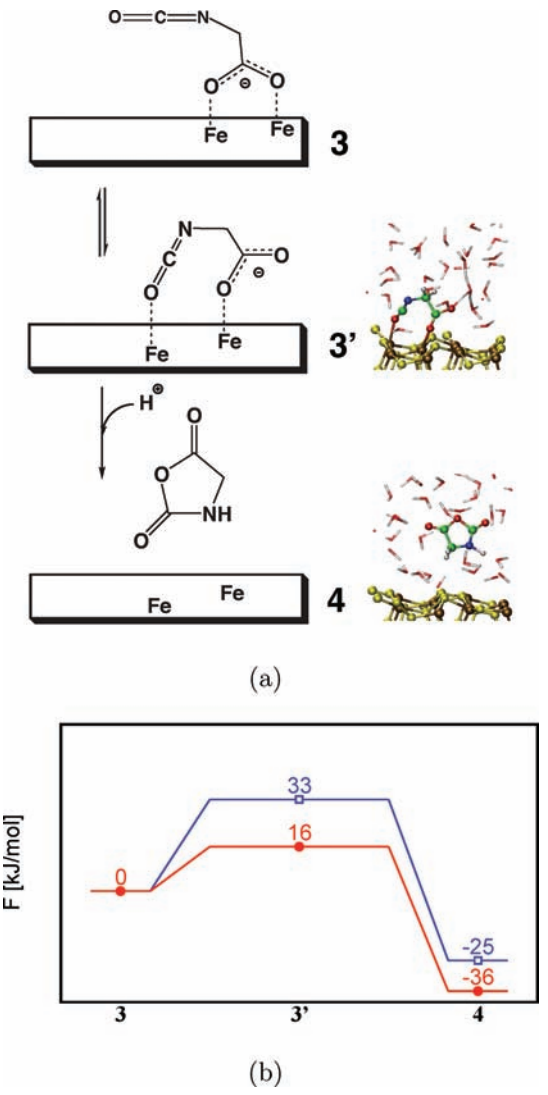

Figure 6. Cyclization of isocyanate at the water−pyrite interface at extreme thermodynamic conditions: (a) reaction mechanism along to the lowest free energy path together with representative snapshots extracted from the ab initio metadynamics simulation. Color code: red (oxygen), green (carbon), white (hydrogen), blue (nitrogen), yellow (sulfur), and brown (iron). (b) Free energy profile along the minimum free energy pathway at the water−pyrite interface at extreme thermodynamic conditions (PIW, red line and filled circles) and in hot-pressurized bulk water at the same conditions (HPW, blue line and open squares). Note that b and thus a are derived from two-dimensional free energy surfaces (see Figure S5, Supporting Information).

In the simulation, as shown in the corresponding snapshot (see Figure 6a), the isocyanate oxygen of **3** strongly attaches to an iron atom yielding **3′** at the expense of detaching one of the two carboxylate oxygens. This expedites greatly the cyclization together with the protonation of nitrogen in a concerted fashion. Clearly, **3′** preforms a cyclic structure (noting that the $C_{iso}-O_{carbox}$ distance is about 2.3 Å) that tremendously facilitates formation of the cyclic topology of adsorbed NCA **4** (see Figure 6), which readily desorbs resulting in a solvated **4** molecule. This chemical scaffolding effect due to the surface, which is distinctly different from the entropic effect observed earlier (compare section 3.1), is responsible for lowering the reaction free energy barrier of this step by a factor of 2 (16 kJ/mol or 4 k_BT_{500} at PIW conditions) in comparison to HPW (33 kJ/mol or 8 k_BT_{500} taken from ref 55). Reducing the reaction barrier by a factor of 2 is a clear sign of the catalytic role of the pyrite surface. It is observed that the reaction does not take place at the defect site itself and that relaxation effects of this defective pyrite surface are rather small,[40] which suggests that also the defect-free (100) surface will greatly accelerate the formation of **3′**.

3.3. Formation of the Peptide Bond. The reactions considered so far generate an activated amino acid in the form of the NCA **4**. In a next step, **4** can react with a peptide or a free amino acid, like in the present case, to form longer peptides according to route D in Figure 1. The chosen subspace to describe this elongation reaction is spanned by three coordinates and is identical to that chosen in ref 55 to investigate this reaction in bulk water. Apart from the distance between the nitrogen atom of glycine and the C5 carbon atom of NCA, $d[N_{Gly}-C5_{NCA}]$, the distance between the oxygen and carbon atom within the NCA, $d[O1_{NCA}-C5_{NCA}]$, and the coordination number of N_{Gly} to *all* nonaliphatic hydrogen atoms, $c[N_{Gly}-H_{na}]$, was taken into account. Again, a repulsive wall potential was set along $c[N_{Gly}-H_{na}]$ at a value of two as to prevent an additional protonation of the amino group. Additionally the distance $d[N_{Gly}-C5_{NCA}]$ was restricted to values smaller than 5 Å, thus preventing separation of the reactants via trivial diffusive processes.

3.3.1. Elongation at the Ideal Pyrite Surface. Within this setup we first investigated peptide bond formation using the ideal pyrite surface. In the starting configuration, both NCA and glycine are adsorbed in a bidentate fashion. In particular, the glycine molecule interacts directly with the surface via its carboxyl group (structure **5**), while the NCA molecule is bound by two of its oxygen atoms to iron atoms of pyrite. The latter adsorption mode is stable only for some picoseconds (during the equilibration). Interestingly, the NCA molecule after desorption is kept near the pyrite surface by hydrogen bonds to water molecules adsorbed at iron centers of the surface (structure **4**) and thus immobilized, which is a "water-mediated adsorption mode" in the interfacial region.

Since (i) the attack of the nitrogen atom of **5** at the C5 atom of **4**, (ii) the ring-opening event, and (iii) the deprotonation at the nitrogen of the formed adduct **5.1** are observed to happen in a more or less concerted way (see Figure 7a), no separate minima could be identified in the reconstructed free energy hypersurface (presented in the Supporting Information, Figure S6). As observed previously, the presence of the surface decreases the effective activation barrier for the entire process, in this case by about one-third to 68 kJ/mol (16 k_BT_{500}) relative to the situation in bulk (Figure 7b).[56] The reason for this effect is again found in the decrease of entropic contributions due to the reduction of the dimensionality of the reaction space. While in HPW solution the two reaction partners can freely rotate relative to each other, at PIW conditions both are more or less immobilized at the surface. In addition, the solvation shell, which interacts with the surface and plays an important role during the deprotonation process, is also less dynamic compared to the bulk situation. A complete free energy sampling of the product basin was not performed, but the product is at least more than 100 kJ/mol more stable than the reactants which allows clear-cut conclusions to be drawn as to the relative stabilities of reactants versus products.

Upon further refining this free energy surface, thus necessarily increasing the generated trajectory length, both reactants were found to desorb from the surface, leaving the reactive interfacial

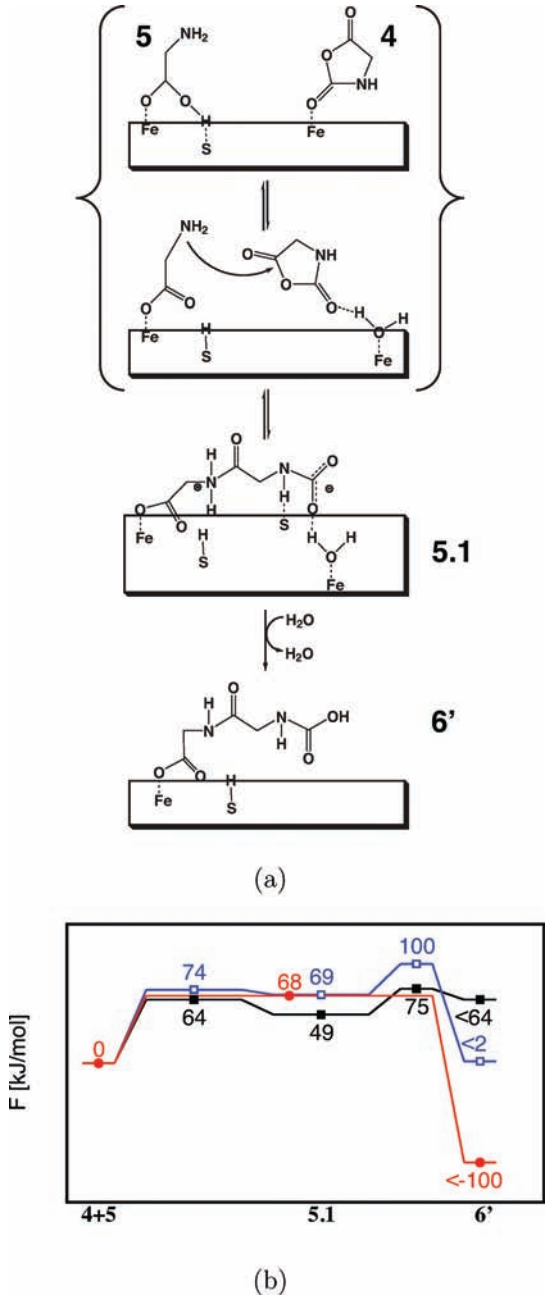

Figure 7. (a) Mechanism for the reaction of glycine with glycine−NCA at the water−pyrite interface at extreme thermodynamic conditions (PIW, see text). (b) Free energy profile along the minimum free energy pathway at the water−pyrite interface at extreme thermodynamic conditions on an ideal pyrite surface (red line and filled circles), on a defective pyrite surface (see text, black line and filled squares), and in hot-pressurized bulk water at the same conditions (HPW, blue line and open squares). Note that b and thus a are derived from three-dimensional free energy surfaces (see Figure S6, Supporting Information).

zone. As discussed before, this is due to the short retention times of such adsorbates on a solvated nondefective pyrite (100) surface. In view of this finding and keeping in mind that sulfur defects have been shown previously[40] to provide an increased stability and thus significantly longer retention times we considered the same reaction on a FeS_2(100) surface with two surface vacancies.

3.3.2. Elongation at Defective Pyrite Surfaces. In the starting configuration on the defective surface, the NCA oxygen at C(2) is bound to one of the four-fold-coordinated Fe atoms near one of the two sulfur vacancies. The two deprotonated carboxylate oxygens of glycine were anchored on five- and four-fold-coordinated Fe atoms in the vicinity of the vacancy with the amino group pointing toward the bulk solution. During the sampling time (corresponding to 30 ps) of the ab initio metadynamics simulation the surface coordination of both adsorbates was retained, in stark contrast to the ideal case. This shows that the defects have indeed increased the retention time of the adsorbates, in qualitative accordance with our earlier conclusions[40] using a different system.

The free energy profile of this reaction is shown in Figure 7b using the same collective coordinates as in the case of the ideal surface. The mechanism of the chemical reaction is the same as the one observed on the ideal surface. The barrier for addition of NCA and glycine to form **5.1** is about 64 kJ/mol, which is nearly the same as that on the ideal surface. Different from the ideal surface, addition of **4** and **5** and deprotonation at the nitrogen in **5.1** leading to **6′** are observed as stepwise processes, thus leading to an intermediate separated by a rather shallow free energy barrier. The deprotonation step occurred after crossing a barrier of about 26 kJ/mol, which is similar to that determined at HPW conditions in the bulk.[56] Thus, the effective barrier for peptide bond formation reaction is 75 kJ/mol at the given reaction conditions.

It is clear that the major role of the surface defects in this reaction is to immobilize the reactant molecules rather than directly affecting the chemical reaction as found in a previous step. Thus, as long as glycine is anchored on the surface there should not be any significant free energy barrier difference for this chemical reaction occurring on an ideal or a defective surface. This nicely explains the similarity of the barrier for the reaction **4** + **5** → **5.1** on ideal and defective pyrite surfaces. Still, it must be kept in mind that only defective surfaces retain the reactants long enough to allow for reactive encounters.

3.4. Back Reaction: Hydrolysis of Diglycine. Finally, we scrutinize the hydrolysis mechanism of the thus "synthesized" dipeptide molecule on the defective pyrite surface (marked as step E in Figure 1). It is recalled that in bulk water at extreme conditions, HPW, the hydrolysis of this peptide was found to be slower than all the steps leading to it.[55,56] However, it is well conceivable that the mineral surface might also catalyze the back reaction. On the other hand, the surface could alternatively protect the peptide from hydrolysis by screening it from solvation and thus from water attack.

In an effort to address the role a pyrite surface might play in peptide hydrolysis, be it accelerating or decelerating, we launched an ab initio metadynamics starting from the final configuration **6** as a result of our previous "virtual synthesis". Here, the diglycine is in its zwitterionic form with one of the carboxylate oxygen atoms pointing axially to an iron atom neighboring the sulfur defect. The amino group is seen to form hydrogen bonds with the three-fold-coordinated surface sulfur atoms. In order to explore the chemically relevant reaction space, we chose three collective coordinates, namely, the distance of the peptide bond, $d[N-C]$, the coordination number of the peptide group nitrogen atom to *all* nonaliphatic hydrogen atoms, $c[N_{pept}-H_{na}]$, and the coordination number of peptide carbon atom to *all* oxygen atoms except those of the carboxyl group, $c[C_{pept}-O_{free}]$. As the reaction progresses, $d[N-C]$ is expected to increase, thus separating the nascent glycine molecules. Furthermore, the two

dx.doi.org/10.1021/ja111503z | J. Am. Chem. Soc. 2011, 133, 8216–8226

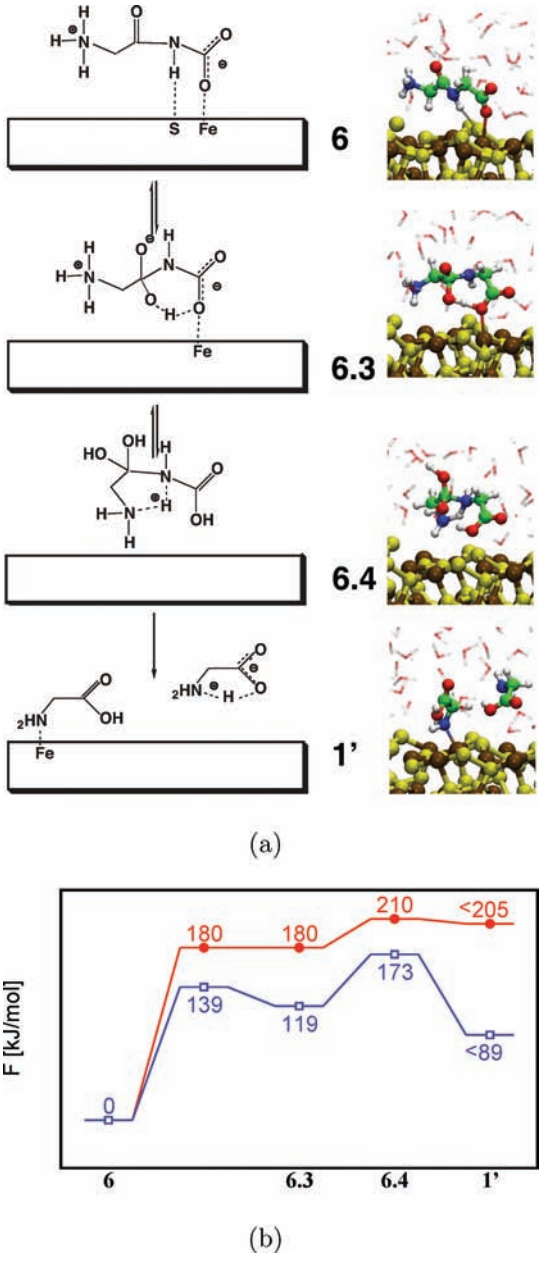

Figure 8. (a) Mechanism of diglycine hydrolysis at the defective pyrite surface at extreme thermodynamic conditions (PIW) together with representative snapshots extracted from the ab initio metadynamics simulation. Color code: red (oxygen), green (carbon), white (hydrogen), blue (nitrogen), yellow (sulfur), and brown (iron). (b) Free energy profile along the minimum energy pathway for diglycine hydrolysis at the water−pyrite interface at extreme thermodynamic conditions (PIW, red line with filled circles) and in hot-pressurized bulk water at the same conditions (HPW, blue line and open squares). Note that b and thus a are derived from three-dimensional free energy surfaces (see Figure S7, Supporting Information).

coordination numbers are expected to increase in the final products by unity in case $c[C_{pept}-O_{free}]$ and by 1 or 2 for $c[N_{pept}-H_{na}]$. The full reaction mechanism obtained, along with the resulting free energy profile for the hydrolysis of diglycine **6** on a pyrite surface, is shown in Figure 8.

A wealth of distinct configurational states of the hydrolyzing system have been sampled during extensive metadynamics sampling. We observed structures which were results of deprotonations of the peptide nitrogen site not only by water molecules as in bulk environments but also by the three-fold-coordinated surface sulfur atom available as a proton acceptor site in the interfacial region. These metastable species were 124 and 72 kJ/mol higher in free energy compared to **6**, respectively, and relaxed without any barrier back to the starting configuration, thus not leading to any productive channels. Instead, hydrolysis progresses through an attack of a water molecule at the peptide carbon atom, leading to species **6.3**. This intermediate state is 180 kJ/mol higher than **6** and represents a high-lying energy plateau on the free energy hypersurface. The respective structure also features a strong hydrogen bond between the attacked water and the carboxylate oxygen atom. This interaction results in weakening the Fe−carboxylate oxygen coordination and thus results in partial desorption of the dipeptide from the surface. Subsequently, the proton is found to move from the attacked water to the carboxylate oxygen, resulting in **6.4**. In an intramolecular reaction a proton is transferred from the terminal amino group to the nitrogen of the peptide, breaking the diglycine into two glycine molecules (structure **1′**). The free energy barrier for the peptide hydrolysis is about 210 kJ/mol. Interestingly, the revealed mechanism is very similar to that in hot-pressurized bulk water reported earlier,[56] but the barrier is 37 kJ/mol ($9\ k_BT_{500}$) *higher* in the present case.

An analysis of the trajectory indicates that attack by water molecules is highly hindered due to the screening effect of the surface. For a nucleophilic attack, the water molecule has to approach the peptide carbon from a particular angle, while in bulk a water can approach from all sides. These restraints on successful configurations for attack result in a higher free energy barrier for hydrolysis at the pyrite−water interface compared to that in HPW.

4. CONCLUSIONS AND OUTLOOK

Using ab initio molecular dynamics techniques supplemented with enhanced sampling we studied the impact of pyrite surfaces, both ideal and defective ones, on the full sequence of reaction step leading to formation of a peptide bond in aqueous environments at elevated temperature and pressure conditions starting from two bare amino acids. Using the "virtual synthesis" of diglycine as the simplest example, various multidimensional free energy landscapes have been generated. They not only provide the reaction barriers at finite temperature and pressure at a fully solvated mineral interface but also allow one to *extract* the detailed reaction mechanism including the net influence of the liquid−solid interface thereupon.

In most cases, it has been observed that pyrite surface aids in expediting the reactions by decreasing the barriers substantially. This is achieved in various ways, namely, (i) by decreasing the fluctuations as a result of immobilizing the reactants on the surface for long enough times, (ii) by preforming and stabilizing transition state structures due to scaffolding imprinted by adsorption sites, and (iii) by directly participating actively in chemical reactions via coordination of a proton or hydride and stabilizing hydrogen bonding interactions. Interestingly, the presence of the surface can also increase the barrier for some reactions like the hydrolysis of diglycine by screening the molecule from water, thus hindering hydrolytic attack.

Similar to the situation in both ambient and hot-pressurized bulk water, the rate-determining step in the reaction sequence sketched in Figure 1 is the formation of isocyanate from thiocarbamate. As an interesting, albeit an exotic, possibility we explored a mechanism for

this step involving a hydride transfer, which turned out to have the smallest free energy barrier for this step among the investigated mechanisms. Of utmost importance is the finding that, compared to the situation in bulk water, the pyrite surface speeds up the formation of isocyanate, i.e., the rate-limiting step on the way from glycine to its homodipeptide, while it simultaneously slows down the hydrolysis of the peptide bond, thus indicating a potentially more productive environment for peptide formation.

These results could shed light on the feasibility of such complex peptide bond formation cycles at prebiotic conditions as relevant to the "iron−sulfur world" hypothesis among others as sketched in the Introduction. Yet our findings are still fairly limited, despite the significant methodological and computational effort invested, given the essentially unlimited scope of "origin of life" issues offering a broad spectrum of ideas, speculations, hypotheses, or even possible side reactions within the same hypothesis. In fact, several side reactions involving the intermediates in the peptide synthesis cycle is critical in judging the feasibility of peptide synthesis at hot-pressurized thermodynamic conditions. More specfically, it is important to consider the hydrolysis of COS, NCA, and the formation of a urea-like compound **7** by reaction of glycine and isocyanate, since they both are expected to influence the concentration of the key NCA molecule. Although the availability of COS is critical to the whole cycle, COS hydrolysis is only important at equilibrium conditions. However, since COS gas is present in hydrothermal exhalations there is a steady supply of COS to the reaction system. Our preliminary calculations of the other two reactions at HPW conditions show that the effective free energy barriers for both side reactions in hot-pressurized conditions are about 100 kJ/mol (see Supporting Information for more details). This barrier is similar to that observed for the reaction between NCA and glycine in hot-pressurized water. Thus, it is clear that peptide-bond formation and hydrolysis of NCA do compete at HPW conditions. The presence of pyrite is not expected to accelerate the hydrolysis of NCA: in the studied hydrolysis of the dipeptide, the surface rather increases the barrier by screening the molecule from water, i.e., the surface stabilizes the peptide. Taking into account that the barrier for peptide-bond formation at PIW conditions is lower (68−75 kJ/mol), suggesting a preference for the system to go along the route of peptide-bond formation. It is not clear how the surface would influence the reaction between glycine and isocyanate. Clearly, more extensive investigations of side reactions are necessary.

Transcending the implications for the origin of life hypotheses, however, the basic results revolving around the impact of both minerals and elevated temperature and pressure conditions on a variety of elementary reactions, widespread in aqueous organic chemistry, will be valuable for (bio)geochemistry, biomineralization, or environmental chemistry to name but a few where wet mineral surfaces and nonambient thermodynamic conditions are key.

■ ASSOCIATED CONTENT

Supporting Information. Reconstructed free energy hypersurfaces for all of the discussed reactions as well as descriptions of the mechanisms of the side reactions. This material is available free of charge via the Internet at http://pubs.acs.org.

■ AUTHOR INFORMATION

Corresponding Author
eduard.schreiner@theochem.rub.de

Present Addresses
[†]Theoretical and Computational Biophysics Group, Beckman Institute, Urbana, IL 61801.
[‡]Department of Chemistry, Indian Institute of Technology, Kanpur 208016, India.

■ ACKNOWLEDGMENT

It gives us pleasure to thank P. McGill for his help with explorative simulations as well as G. Wächtershäuser and H. R. Kricheldorf for stimulating discussions at at an early stage of the project. Partial financial support was provided by DFG (Normalverfahren MA 1547/7), RD IFSC, and FCI. The simulations were carried out on the IBM Blue Gene system at John von Neumann Institute for Computing (NIC) at Forschungszentrum Jülich (Germany).

■ REFERENCES

(1) Kricheldorf, H. R. *α-Aminoacid-N-Carboxy-Anhydrides and Related Hetrocycles*; Springer-Verlag: New York, 1987.
(2) Kricheldorf, H. R. *Angew. Chem., Int. Ed.* **2006**, *45*, 5752–5784.
(3) Deming, T. J. *Adv. Polym. Sci.* **2006**, *202*, 1–18.
(4) Deming, T. J. *Prog. Polym. Sci.* **2007**, *32*, 858–875.
(5) Collet, H.; Bied, C.; Mion, L.; Taillades, J.; Commeyras, A. *Tetrahedron Lett.* **1996**, *37*, 9034–9046.
(6) Commeyras, A.; Collet, H.; Boiteau, L.; Taillades, J; Vandenabeele-Trambouze, O.; Cottet, H.; Biron, J.-P.; Plasson, R.; Mion, L.; Lagrille, O.; Martin, H.; Selsis, F.; Dobrijevic, M. *Polym. Int.* **2002**, *51*, 661–665.
(7) Huber, C.; Wächtershäuser, G. *Science* **1998**, *281*, 670–672.
(8) Leman, L.; Orgel, L.; Ghadiri, M. R. *Science* **2004**, *306*, 283–286.
(9) Pascal, R.; Boiteau, L.; Commeyras, A. *Top. Curr. Chem.* **2005**, *259*, 69–122.
(10) Leman, L. J.; Orgel, L. E.; Ghadiri, M. R. *J. Am. Chem. Soc.* **2006**, *128*, 20–21.
(11) Biron, J.-P.; Parkes, A. L.; Pascal, R.; Sutherland, J. D. *Angew. Chem., Int. Ed.* **2005**, *44*, 6731–6734.
(12) Huber, C.; Eisenreich, W.; Hecht, S.; Wächtershäuser, G. *Science* **2003**, *301*, 938–940.
(13) Wächtershäuser, G. *Microbiol. Rev.* **1988**, *52*, 452–484.
(14) Wächtershäuser, G. *Prog. Biophys. Mol. Biol.* **1992**, *58*, 85–201.
(15) Lambert, J. F. *Origins Life Evol. Biospheres* **2008**, *38*, 211–242.
(16) Ohara, S.; Kakegawa, T.; Nakazawa, H. *Origins Life Evol. Biospheres* **2007**, *37*, 215–223.
(17) Saladino, R.; Neri, V.; Crestini, C.; Costanzo, G.; Graciotti, M.; Mauro, E. D. *J. Am. Chem. Soc.* **2008**, *130*, 15512–15518.
(18) Mateo-Marti, E.; Briones, C.; Rogero, C.; Gomez-Navarro, C.; Methivier, C.; Pradier, C. M.; Martin-Gago, J. A. *Chem. Phys.* **2008**, *352*, 11–18.
(19) Nesbitt, H. W.; Bancroft, G. M.; Pratt, A. R.; Scaini, M. J. *Am. Mineral.* **1998**, *83*, 1067.
(20) Guevremont, J. M.; Elsetinow, A. R.; Strongin, D. R.; Bebie, J.; Schoonen, M. A. A. *Am. Mineral.* **1998**, *83*, 1353–1356.
(21) Eggleston, C. M.; Ehrhardt, J.-J.; Stumm, W. *Am. Mineral.* **1996**, *81*, 1036–1056.
(22) Rosso, K. M.; Becker, U.; Hochella, M. F., Jr. *Am. Mineral.* **1999**, *84*, 1535–1548.
(23) Garvie, L. A. J.; Buseck, P. R. *Am. Mineral.* **2004**, *89*, 485–491.
(24) Zeng, Y.; Holzwarth, N. A. W. *Phys. Rev. B* **1994**, *50*, 8214–8220.
(25) Eyert, V.; Höck, K.-H.; Fiechter, S.; Tributsch, H. *Phys. Rev. B* **1998**, *57*, 6350–6359.
(26) Opahle, I.; Koepernik, K.; Eschrig, H. *Phys. Rev. B* **1999**, *60*, 14035–14041.
(27) Gerson, A. R.; Bredow, T. *Surf. Interface Anal.* **2000**, *29*, 145–150.

(28) de Leeuw, N. H.; Parker, S. C.; Sithole, H. M.; Ngoepe, P. E. *J. Phys. Chem. B* **2000**, *104*, 7969–7976.
(29) Muscat, J.; Hung, A.; Russo, S.; Yarovsky, I. *Phys. Rev. B* **2002**, *65*, 054107–1−12.
(30) Hung, A.; Muscat, J.; Yarovsky, I.; Russo, S. P. *Surf. Sci.* **2002**, *513*, 511.
(31) Guanzhou, Q.; Qi, X.; Yuehua, H. *Comput. Mater. Sci.* **2004**, *29*, 89.
(32) Cai, J.; Philpott, M. R. *Comput. Mater. Sci.* **2004**, *30*, 358.
(33) Stirling, A.; Bernasconi, M.; Parrinello, M. *Phys. Rev. B* **2007**, *75*, 165406.
(34) Boehme, C.; Marx, D. *J. Am. Chem. Soc.* **2003**, *125*, 13362–13363.
(35) Stirling, A.; Bernasconi, M.; Parrinello, M. *J. Chem. Phys.* **2003**, *118*, 8917–8926.
(36) Stirling, A.; Bernasconi, M.; Parrinello, M. *J. Chem. Phys.* **2003**, *119*, 4934–4939.
(37) Hung, A.; Yarovsky, I.; Russo, S. P. *J. Chem. Phys.* **2003**, *118*, 6022.
(38) Philpott, M. R.; Goliney, I. Y.; Tin, T. T. *J. Chem. Phys.* **2004**, *120*, 1943–1950.
(39) Pollet, R.; Boehme, C.; Marx, D. *Origins Life Evol. Biospheres* **2006**, *36*, 363–379.
(40) Nair, N. N.; Schreiner, E.; Marx, D. *J. Am. Chem. Soc.* **2006**, *128*, 13815–13826.
(41) Luck, J.; Hartmann, A.; Fiechter, S. *Fresenius Z. Annal. Chem.* **1989**, *334*, 441–446.
(42) Birkholz, M.; Fiechter, S.; Hartmann, A.; Tributsch, H. *Phys. Rev. B* **1991**, *43*, 11926–11936.
(43) Andersson, K.; Nyberg, M.; Ogasawara, H.; Nordlund, D.; Kendelewicz, T.; Doyle, C. S.; Brown, G. E., Jr.; Pettersson, L. G. M.; Nilsson, A. *Phys. Rev. B* **2004**, *70*, 195404.
(44) Murphy, R.; Strongin, D. R. *Surf. Sci. Rep.* **2009**, *64*, 1–45.
(45) Amend, J. P.; Shock, E. L. *Science* **1998**, *281*, 1659–1662.
(46) Imai, E.; Honda, H.; Hatori, K.; Brack, A.; Matsuno, K. *Science* **1999**, *283*, 831–833.
(47) Singh, S. C.; Crawford, W. C.; Carton, H.; Seher, T.; Combier, V.; Cannat, M.; Canales, J. P.; Düsünür, D.; Escartin, J.; Miranda, J. M. *Nature* **2006**, *442*, 1029–1032.
(48) Rimola, A.; Sodupe, M.; Ugliengo, P. *J. Am. Chem. Soc.* **2007**, *129*, 8333–8344.
(49) Arrouvel, C.; Diawara, B.; Costa, D.; Marcus, P. *J. Phys. Chem. B* **2007**, *111*, 18164–18173.
(50) Irrera, S.; Costa, D.; Mucus, P. *J. Mol. Struct. THEOCHEM* **2009**, *903*, 49–58.
(51) Mignon, P.; Ugliengo, P.; Sodupe, M. *J. Phys. Chem. C* **2009**, *113*, 13741–13749.
(52) Weingärtner, H.; Frank, E. U. *Angew. Chem., Int. Ed.* **2005**, *44*, 2672–2692.
(53) Marx, D.; Hutter, J. *Ab Initio Molecular Dynamics: Basic Theory and Advanced Methods*; Cambridge University Press: Cambridge, 2009.
(54) Schreiner, E.; Nair, N. N.; Marx, D. *J. Am. Chem. Soc.* **2008**, *130*, 2768–2770.
(55) Nair, N. N.; Schreiner, E.; Marx, D. *J. Am. Chem. Soc.* **2008**, *130*, 14148–14160.
(56) Schreiner, E.; Nair, N. N.; Marx, D. *J. Am. Chem. Soc.* **2009**, *131*, 13668–13675.
(57) Perdew, J. P.; Burke, K.; Ernzerhof, M. *Phys. Rev. Lett.* **1996**, *77*, 3865–3868.
(58) Perdew, J. P.; Burke, K.; Ernzerhof, M. *Phys. Rev. Lett.* **1997**, *78*, 1396–1396.
(59) Vanderbilt, D. *Phys. Rev. B* **1990**, *41*, 7892–7895.
(60) Car, R.; Parrinello, M. *Phys. Rev. Lett.* **1985**, *55*, 2471–2474.
(61) Martyna, G. J.; Klein, M. L.; Tuckerman, M. *J. Chem. Phys.* **1992**, *97*, 2635–2643.
(62) Lown, D. A.; Thirsk, R. H.; Lord Wynne-Jones *Trans. Faraday Soc.* **1970**, *66*, 51–73. Note: the typographical error in the specific volume of 1.1178 cm^3/g for 200 bar pressure and 225 °C temperature in Table 5 (page 62) is corrected to 1.1778 cm^3/g.
(63) Iannuzzi, M.; Laio, A.; Parrinello, M. *Phys. Rev. Lett.* **2003**, *90*, 238302−1–4.
(64) Laio, A.; Parrinello, M. *Proc. Natl. Acad. Sci.* **2002**, *99*, 12562–12566.
(65) *CPMD*, Version 3.13.1; *IBM Corp.*, Rüschlikon, 1990−2010; MPI für Festkörperforschung: Stuttgart, 1997−2001. See also http://www.cpmd.org.
(66) Raiteri, P.; Laio, A.; Gervasio, F. L.; Micheletti, C.; Parrinello, M. *J. Phys. Chem. B* **2005**, *110*, 3533.
(67) Nair, N. N.; Schreiner, E.; Marx, D. *In* Rainer, F., Ed., *inSiDE*, Vol. 6; pp 30−35; HLRS, Stuttgart, Germany, 2008; http://inside.hlrs.de/htm/Edition_02_08/article_09.html
(68) Ensing, B.; Laio, A.; Parrinello, M.; Klein, M. L. *J. Phys. Chem. B* **2005**, *109*, 6676–6687.